An experimental and modeling investigation of the combustion of anisole and guaiacol

N. Delort, I. Meziane, M. Framinet, R. Bounaceur, Jérémy Bourgalais, Frederique Battin-Leclerc, Olivier Herbinet

AN EXPERIMENTAL AND MODELING INVESTIGATION OF THE COMBUSTION OF ANISOLE AND GUAIACOL

N. Delort, I. Meziane, M. Framinet, R. Bounaceur, J. Bourgalais, F. Battin-Leclerc*, O. Herbinet

Université de Lorraine, CNRS, LRGP, F-54000 Nancy, France

Paper published in Fuel, Volume 362, 15 April 2024, 130832
https://doi.org/10.1016/j.fuel.2023.130832

ABSTRACT

Anisole and guaiacol are both used as surrogates for lignin-derived biofuels. However, while the oxidation reaction mechanisms of anisole can be validated against a large set of experimental data, experimental measurements and models for guaiacol are limited. In this context, in addition to measuring adiabatic laminar burning velocities of both fuels using a flat flame burner, the oxidation of guaiacol was investigated at temperatures between 600 and 925 K. A near-atmospheric pressure jet-stirred reactor was used for three equivalence ratios (0.5, 1 and 2) with a high helium dilution. The experiments yielded mole fractions of 22 reaction products, among which two new species, benzodioxole and benzodioxole-2-one, were identified. All the measurements made in this work, along with extensive literature data on anisole, were compared with the predictions of a newly developed kinetic model. A good agreement was found between kinetic modeling and experiments, showing improved prediction for some species relative to the existing literature guaiacol oxidation models. Flow-rate analyses are also discussed both in flames and in the jet-stirred reactor, especially focusing on the formation of the newly detected products.

Keywords: oxidation; guaiacol; biomass; jet-stirred reactor; kinetic modeling

* *Corresponding author: frederique.battin-leclerc@univ-lorraine.fr.*

1. INTRODUCTION

Due to its abundance and availability, biomass is a promising alternative fuel for energy conversion systems to address fossil fuel reliance. However, the transition from fossil fuels to sustainable energy sources is a challenge for industrial processes that rely on the intrinsic physicochemical properties of biomass, such as gasification or combustion. Biomass contains higher contents of oxygen and volatile organic matter than coal and oil, which makes it more susceptible to char formation and resulting operational issues like coke deposit and catalyst deactivation [1,2].

Lignin, the second most abundant component of lignocellulosic biomass, is mostly considered as a waste in processes using cellulose. However, through reductive catalytic lignin solvolysis, it can be transformed into commercially viable products, such as biofuels [3]. This is a focus of study in the EHLCATHOL European project (http://ehlcathol.eu/).

Lignin is mainly composed of oxygenated phenyl-propane units. Its decomposition yields oxygenated aromatics (e.g. anisole, guaiacol, syringol, cresol), which are considered representative surrogate biofuels obtained from lignin [3]. Understanding the elementary chemical reactions and the corresponding kinetic parameters of these oxygenated aromatics is crucial for modeling the reactions of tars produced during biomass pyrolysis.

The pyrolysis and oxidation of anisole, the simplest methoxy-bearing aromatic compound, have been thoroughly investigated through laboratory experiments focusing on various parameters like laminar burning velocities [4–6] and ignition delay times [7,8], as well as species profiles in shock tubes [9,10], tubular reactors [11–16], jet-stirred reactors (JSRs) [4,17–19] and in laminar flames [20,21]. These experimental data have led to the development of several detailed kinetic models [4,7,12,18], elucidating the chemistry of methoxy aromatics.

On its side, ortho-guaiacol (2-methoxyphenol) has so far received much less attention despite being more representative of lignin structure and a more appropriate substitute for lignin-derived biofuels [3] and primary tars from lignin pyrolysis [3,22,23]. Although some studies concerned its pyrolysis [24–28], so far only one experimental study focused on the oxidation of guaiacol [28] (this was made using a JSR) and none on its laminar burning velocity (LBV). The low number of studies about the guaiacol kinetics in combustion might be due to its low volatility (T_{boil}= 478 K) and high melting temperature (T_{melt} = 301 K) [3]. However, its global combustion performance indicators are excellent. Relatively to a volume unit, the Lower Heating Value (LHV) of guaiacol, 31 MJ/L, is just a little bit lower than that of petroleum derived fuels (≈ 33 MJ/L) despite the presence of two O-atoms [3]. The Research Octane Number (RON) of guaiacol has never been experimentally measured, but it is expected to be higher than 100, like other aromatics, arenes, and oxygenated ones [3]. Finally, aromatics are known as soot precursors, but those containing two O-atoms, like guaiacol and catechol, have a far lower Yield Sooting Index (e.g., $YSI_{o\text{-}guaiacol}$= 64) than their counterparts with zero and one O-atom [3], indicating a lower propensity to produce soot.

In the guaiacol oxidation study conducted using a JSR by Nowakowska et al. [28], a gas mixture (He/guaiacol/O_2) with an equivalence ratio (ϕ) of 1 was continuously fed into the heated quartz sphere under near atmospheric pressure with a residence time of 2 s. The JSR was connected to gas chromatographs (GCs) to quantify fuel and stable products as a function of the reactor temperature that was varied between 623 and 923 K. The paper by Nowakowska et al. [28] displayed the mole fractions of 24 species with the most abundant ones being CO, methane, ethylene, hydrogen, and phenolic molecules (e.g. phenol, pyrocatechol, 2-hydroxybenzaldehyde, and methylcatechols). By comparison with their previous work on anisole using the same experimental set-up [18], they showed that the addition of an -OH group makes the consumption of guaiacol to start 100 K lower due to a 5 kcal/mol decrease in the O-CH_3 bond dissociation energy (58.1 kcal.mol^{-1} for guaiacol and 63.2 kcal.mol^{-1} for anisole). To understand the chemistry of guaiacol oxidation, they developed a kinetic model based on their previous model of anisole [18], which was validated by comparison against their experimentally measured mole fractions. They found that the decomposition of guaiacol is based on a competition between unimolecular decomposition and H-abstraction from the hydroxy and methoxy groups. The first channel yields catechol and methylcatechols, while the second one leads to phenol and 2-hydroxybenzaldehyde. However, the products from the radical chain mechanism, especially phenol and soot precursors (e.g., benzene, naphthalene), were not well predicted. This is due to a lack of knowledge of the chemistry of these intermediates and more generally poly-substituted phenols, for which more studies are needed to get a complete picture of guaiacol decomposition and other methoxyphenols from biomass.

In order to expand the experimental database concerning anisole and guaiacol, measurements of laminar burning velocity (LBV) using a laminar flame burner were performed, as well as a quantification of the oxidation products obtained in a JSR using the same experimental procedure as Nowakowska et al. [28], but under wider combustion conditions in terms of equivalence ratios. These experimental measurements, as well as literature data, were used to constrain and validate a new kinetic model that has been developed in this work to accurately reproduce the oxidation of anisole and guaiacol on a wide range of temperatures; this model is an extension of that recently published for the oxidation of toluene and xylene isomers [29].

2. EXPERIMENTAL SETS-UPS AND DETAILED KINETIC MODEL

This part aims at describing the two used experimental sets-ups: the laminar flame burner for LBV measurements, and the JSR coupled to GCs used for the quantification of oxidation products. This part also details the newly developed kinetic model for the oxidation of anisole and guaiacol.

2.1. Laminar burning velocity measurements using a laminar flame burner

Adiabatic LBV is measured using a flat flame burner under atmospheric pressure based on the heat-flux method [30]. This apparatus was previously used to measure the LBV of a wide range of liquid fuels, including an aromatic molecule, toluene [31]. Under adiabatic conditions, heat losses and gain

balance each other out, and a flat temperature profile, measured by thermocouples inserted inside the burner plate, is observed. In this case, Bosschaart and de Goey [30] have established that the velocity of the adiabatic flame is equal to the velocity of the gas.

The liquid fuel, stored in a tank, is mixed with artificially reconstituted air (21% O_2 + 79% N_2) before entering an evaporator and being injected into the plenum chamber that is encompassed by a thermostatic oil jacket, the temperature of which is set to the desired initial temperature of the unburned gas mixture, with a maximum temperature of 398 K. Anisole and guaiacol are provided by Merck with purities above 99%. Mass flow controllers are used to regulate gas flow rates, and a Cori-Flow mass flow controller regulates the liquid one. Due to the high melting point of guaiacol (301 K), modifications were necessary compared to the setup used in the study by Dirrenberger et al. [31]. The main modifications concern the inlet feed of reactants. The fuel bottle is kept in a hot water bath until used to fill the stainless-steel tank that feeds the liquid flow controller upstream of the evaporation chamber. Electric heating lines and insulation wrap up the fuel tank and all the lines transferring liquid or gases toward the burner in order to ensure a constant temperature of 353 K from the tank to the evaporator and of 398 K from the evaporator to the burner.

LBV measurements were performed across the broadest range of equivalence ratios (see data in an excel spreadsheet in Supplementary Material (SM) and in Figure 1), for which the flame was stable, and the flame shape is flat in lean mixtures and there was neither liquid condensation at the walls nor cellular instabilities in rich mixtures [32]. The uncertainties displayed in Figure 1 are calculated for each individual experiment and take into account the uncertainties of the flow controllers, of the plate K-type thermocouples, and of the T-type thermocouple measuring the fresh gas temperature in the plenum chamber. The variations of the chamber temperature, consideration of adiabatic conditions, and minor and difficult-to-evaluate sources of uncertainties such as distortion and edge effects also contribute. The main source of uncertainty is the plate K-type thermocouples, which account for between one third and half of the total uncertainty. The total uncertainty reaches 2.5 cm/s (12%, for $\phi = 0.55$ and a temperature at the burner of 398 K) in the anisole lean flame.

2.2. Quantification of oxidation products in a jet-stirred reactor

The heated JSR consists of a 92-cm^3 fused silica sphere, where a guaiacol/O_2/He gaseous mixture is injected through nozzles located at the center of the sphere to provide turbulent jets for efficient mixing. However, this reactor was treated with a solution of boric acid to avoid undesirable catalytic effects of the wall. This solution forms an impervious layer of boron oxide, as already explained by Egerton and Warren [33]. The experimental method used was previously described in detail in the literature (see, for instance, Meziane et al. [29,34]). Thus, only the specificities related to this work are detailed below.

He and O_2 were provided by Messer (both 99.999% pure); guaiacol was purchased from Merck with a purity found to be >99%. Similar to LBV measurements, the guaiacol bottle was kept in a hot water bath until used to fill the stainless-steel tank feeding the liquid flow controller upstream of the

evaporation chamber. The tank and all lines transferring liquid toward the evaporator were wrapped up by electric heating lines and insulations to ensure a constant temperature of 353 K.

The oxidation gas mixture exiting the JSR was transferred via heated lines to three GCs for analysis. Hydrogen could not be detected using the available GCs. The gas leaving the reactor was transported by a heated line toward two GCs. The first GC, equipped with a Carbosphere packed column and a thermal conductivity detector (TCD), was used for the quantification of oxygen. The second GC, fitted with a Q-Bond capillary column and a FID, preceded by a methanizer, was used for the quantification of CO, CO_2, and organic compounds from those containing two carbon atoms, such as acetylene or ethylene, up to compounds with 6 carbon atoms, such as benzene.

Due to the high boiling point of guaiacol (478 K), instead of analyzing the heavy molecules ($>C_6$) after on-line transfer to the GC as for the lighter species, those were cryogenically trapped. The content of the trap was then dissolved in acetone and injected by auto-sampling. A third GC, equipped with a HP-5 capillary column and both a mass spectrometer and a FID detector, was then used for the quantification of these heaviest compounds (C_{6+}). The identification of reaction products was performed using a GC equipped with both types of capillary columns and coupled to a mass spectrometer (GC-MS). Calibrations were performed by injecting standards, when possible, with a maximum relative error in mole fractions around ±5%. Otherwise, the effective carbon number method (ECN) was used, with a maximum relative error in mole fractions of approximately ±10% for products.

The JSR quantified mole fractions are provided in the excel spreadsheet in SM dedicated to experimental results. Table S1 in SM displays the obtained carbon atom balances. The carbon balance is around 100 % (±20%), except at Φ= 2 for some temperatures (T= 825, 875, 900 and 925 K), where the carbon balance is less than 80%, possibly due to the condensation of heavy species. At T= 925 K and Φ= 0.5, the carbon balance is around 50%, probably due to oscillation behavior. As described in several studies on the JSR oxidation of hydrocarbons [29,35], at temperatures where fuel is close to being fully consumed, a transient evolution of species mole fractions with time (oscillations) is observed experimentally and numerically. A carbon balance higher than 100% is due to uncertainties in species mole fractions.

2.3. Detailed kinetic model for the kinetics of anisole and guaiacol

The experimental mole fractions measured during the oxidation of guaiacol were compared to predictions from a new detailed kinetic model named COLIBRI v2 (COmbustion of LIgnin derived Biofuel for Research and Innovation). A first version of this model was developed to reproduce data for the kinetics of toluene and xylenes [29], as well as for anisole and guaiacol. The COLIBRI v2 model includes 471 species and 2889 reactions and is provided in SM along with its thermochemical data and transport data. It combines various sub-mechanisms:

- The Galway reaction base [36] for its accuracy and efficiency in LBV computations.
- The toluene model of Yuan et al. [37] for its accuracy in predicting results for toluene oxidation,

- The xylene model of Kukkadapu et al. [38],
- The anisole model of Buttgen et al. [7], supplemented by that of Wagnon et al. [4] for the reactions of methylanisole and ethylphenol,
- The guaiacol model of Nowakowska et al. [28],
- A mechanism of 1.3-benzodioxole and benzodioxole-2-one.

The changes made to simulate the kinetics of toluene and xylenes were described in [29], and those specific to the kinetics of anisole and guaiacol are detailed in an Excel file in SM. More especially, submechanisms responsible for producing and consuming 1.3-benzodioxole and benzodioxole-2-one were developed as part of this work and are provided in Table S2 in SM.

Thermochemical and transport data for each species are taken from the previously mentioned models where the species was initially considered in reactions. The rate constants of the 1,3-benzodioxole and benzodioxole-2-one sub-mechanisms are determined based on analogies with similar reactions, and the thermodynamic data of the newly involved species are calculated using the RMG online software [39]. Transport data are calculated with an in-house code based on correlations proposed by Wand and Frenklach [40].

For anisole and guaiacol, validations based on literature data are listed in the Table 1 and are presented in SM from Figure S1 to S19.

All simulations described in this work were performed using the CHEMKIN software [41].

Table 1: Validation targets considered for testing the COLIBRI v2 model using recent literature data. In flame studies, the indicated temperature is that of fresh gases.

Target	Exp. set-up	Fuel	T(K)	P(atm)	ϕ	n° Fig.	Ref.
IDT	Shock tube	Anisole	770-1600	10-40	0.5, 1	S1	[8]
			900-1315	10-40	0.5, 1	S2	[7]
	RCM	Anisole	750-900	10-40	0.5-2	S2	[7]
LBV	Flat flame burner	Anisole	358	1	0.6-1.2	1	[4]
	Bunsen burner	Anisole	423	1-7.5	0.6-1.3	S3	[6]
Product profiles	Shock tube	Anisole	1100-1400	0.5-0.8	Pyrolysis	S4	[9]
			1425, 1530	1.5	Pyrolysis	S5	[10]
	JSR	Anisole	675-1175	1.08	Pyrolysis, 1	S6-7	[18]
			770-1250	1	0.5-2	S8-10	[4]
			640-990	0.9	0.4	S11	[17]
		Guaiacol	625-925	1.08	Pyrolysis, 1	S18-19	[28]
	Flow reactor	Anisole	850-1170	0.04-1	Pyrolysis	S12-13	[12]
	Premixed flame	Anisole	300	0.04	1.2, 1.6	S14-15	[20]
	Diffusion flame	Anisole-methane	433 (fuel injector) 313 (ox. injector)	1	1.82	S16-17	[21]

3.

RESULTS AND DISCUSSION

Below, we discuss the newly obtained experimental results and how they compare with the predictions using the newly proposed detailed kinetic model.

3.1. LBV measurements, modeling, and kinetic analysis

As is shown in Figure 1, LBV measurements for anisole were conducted at two burner temperatures, 358 and 398 K, covering a wide range of ϕ values from 0.6 to 1.5 and 0.55 to 1.6, respectively. Due to the low volatility of guaiacol (with a boiling point of 478 K compared to 426 K for anisole), LBV measurements were only feasible at a fresh gas temperature of 398 K and for ϕ values from 0.7 to 0.9, as fuel condensation occurred in the pipes beyond ϕ=0.95. Figure 1a shows that, for guaiacol, it was not possible to reach the LBV maximum. However, these measurements indicate a lower LBV for guaiacol compared to anisole at a given ϕ and temperature.

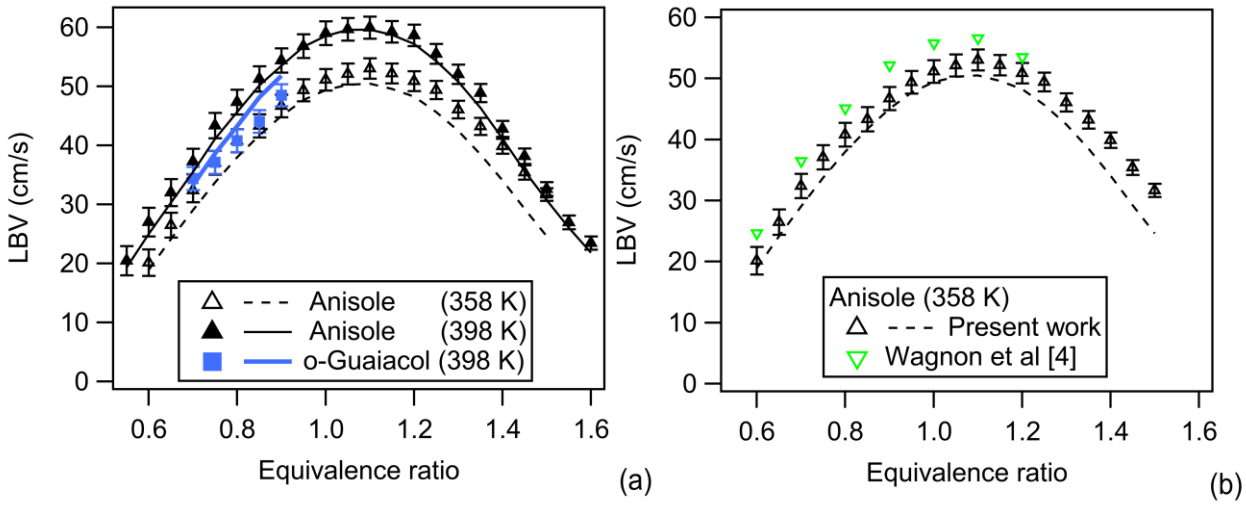

Figure 1: Experimental and simulated LBV of anisole and guaiacol: (a) comparison between experiments and simulation of the present work, (b) comparisons between our measurements for anisole and those of Wagnon et al. [4] at 358 K and 1 bar.

Figure 1b displays a comparison between our measurements for anisole and those made by Wagnon *et al.* [4], also using a flat flame burner, under the same conditions but for a limited range of ϕ, up to 1.2. Both sets of data indicate a maximum LBV value at ϕ = 1.1; however, the value of Wagnon *et al.* [4] is up to 5 cm/s higher, slightly exceeding the reported measurement uncertainty. Figure 1a shows that simulations using the newly developed kinetic model reasonably reproduces the data measured for anisole at the two investigated burner temperatures and for guaiacol at 398 K.

For flames with a fresh gas temperature of 398 K, the flow rate analysis of anisole consumption at ϕ = 0.8 and 1.3 is displayed in Figure 2, and that of guaiacol consumption at ϕ = 0.8 is presented in Figure 3. These are integrated flow rates over the entire flame thickness. Figure 4 presents the most sensitive

reactions involving C_{5+} reactions for the LBV of anisole and guaiacol; sensitivity analyses displaying the ten more sensitive reactions are given in SM (Figures S20-S22).

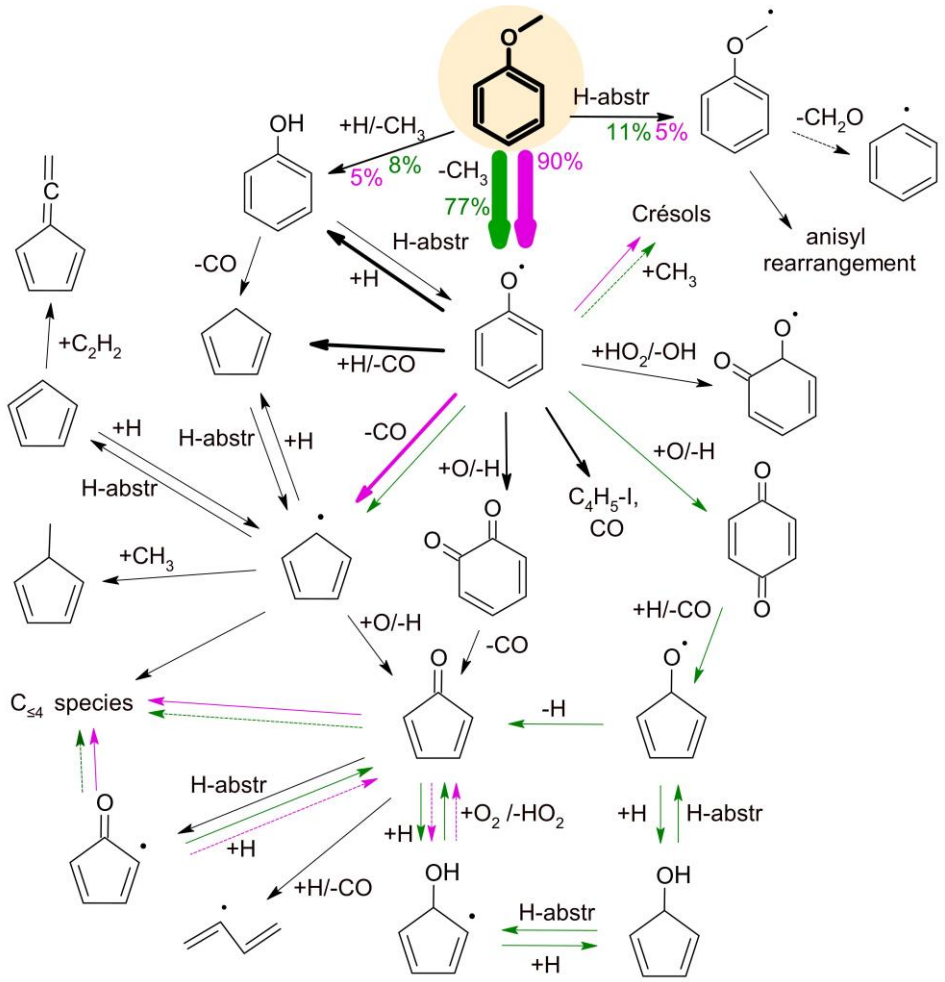

Figure 2: Flow rate analysis in anisole flame at Φ = 0.8 (green arrows) and 1.3 (pink arrows). Black arrows represent common pathways with similar flows. Flow rates are integrated over the flame thickness.

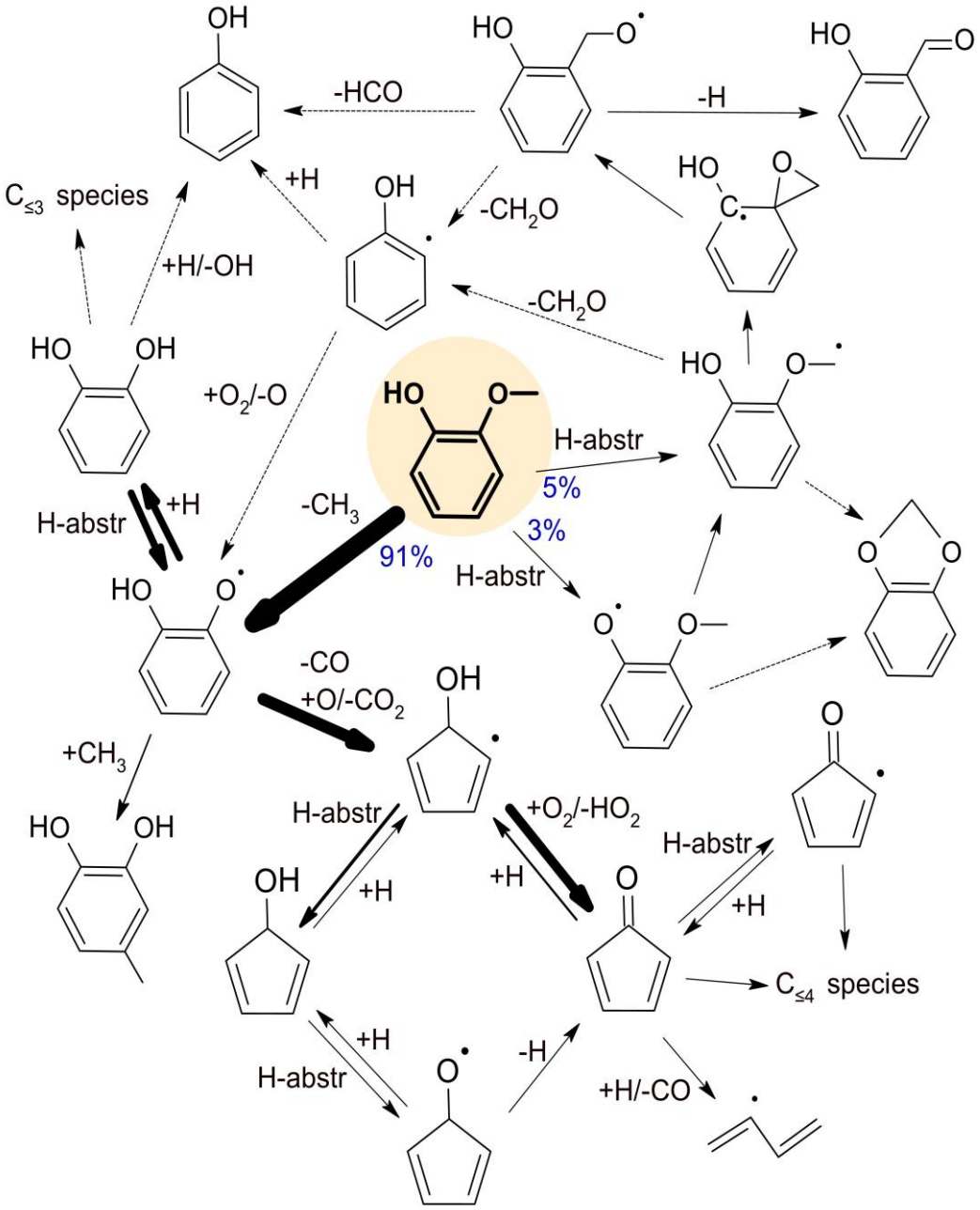

Figure 3: Flow rate analysis in guaiacol flame at $\Phi = 0.8$. Flow rates are integrated over the flame thickness.

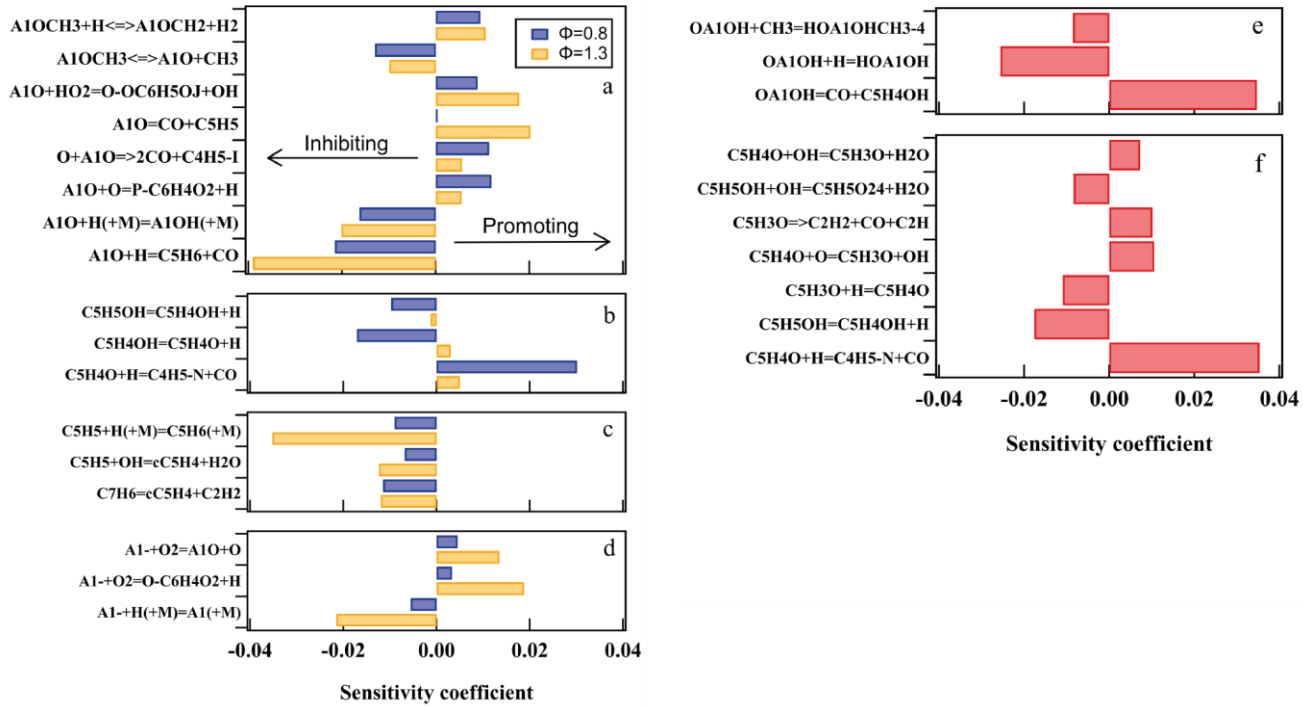

Figure 4: Sensibility analyses (CHEMKIN) for the most sensitive reactions involving C_{5+} reactions for the LBV of anisole at ϕ = 0.8 and 1.3 (a) the reactions involving anisole and phenoxy radicals, (b) the reactions of oxygenated C_5 cyclic species, (c) the reactions of C_5 cyclic hydrocarbons, (d) the reactions involving phenyl radicals, and of guaiacol at ϕ = 0.8 with (e) the reactions involving hydroxyphenoxy radicals, (f) the reactions of oxygenated C_5 cyclic species. The species names are those used in the COLIBRI v2 model.

For both anisole and guaiacol, the main decomposition pathway involves unimolecular decomposition, breaking the O-CH_3 bond and leading to phenoxy and hydroxyphenoxy radicals. The predominance of these unimolecular decompositions is due to the low energy of the O-CH_3 bound, equal to 63.2 kcal/mol [18] for anisole and even lower at 58.1 kcal/mol, as calculated by [28] for guaiacol, resulting in an even higher contribution of this reaction for guaiacol at the same ϕ. Despite involving radical creation, the sensitivity analysis in Figure 4a indicates that the unimolecular decomposition of anisole is an inhibiting pathway, this is because it leads to resonance-stabilized phenoxy radicals, which are involved in termination reactions that consume H-atoms to form stable molecules. In contrast, H-abstractions from anisole promote flame propagation, even when consuming H-atoms. Other fuel consumption pathways, such as H-abstractions on the methoxy group or the hydroxy group in the case of guaiacol, are of lower importance in the flame. Due to their increased importance in JSR conditions, the H-abstraction channels will be discussed in more detail in the next section.

Due to their resonance stabilized behavior, hydroxyphenoxy and phenoxy radicals play an equivalent role in guaiacol and anisole flames and are central to a strong competition between inhibiting and promoting pathways. In the guaiacol flame, the key role of hydroxyphenoxy radicals is highlighted in the guaiacol sensitivity analysis displayed in figure 4e. The reactions consuming them are very sensitive

and include two combinations, with H-atoms and methyl radicals, respectively, appearing as inhibiting pathways because they both form stable molecules: pyrocatechol and methylcatechol. The promoting pathway highlighted in this sensitivity analysis (figure 4e) is the CO-elimination leading to cyclopentadienol radicals. In the same way, the reaction of phenoxy radicals has a determining role during anisole combustion, with the two termination reactions with H-atoms being particularly inhibiting for the two considered ϕ (see Figure 4a). For anisole, the combination with the methyl radical and the CO elimination have a lower impact than for guaiacol. In competition with these inhibiting pathways, the other consumption reactions of phenoxy radicals promote flame propagation.

At ϕ= 0.8, starting from either anisole or guaiacol, the submechanism involving cyclopentadienol radicals (C_5H_4OH and C_5H_5O24), cyclopentadienol (C_5H_5OH), cyclopentadienone (C_5H_4O), and C_5H_3O radicals has a significant inhibiting role (see Figures 4b and 4f). The only pathways allowing exit from this C_5H_XO submechanism involve the consumption of cyclopentadienone, either to produce its radical C_5H_3O through an H-abstraction or to produce smaller linear species. Therefore, these reactions are promoting pathways in the sensitivity analyses, and the reaction leading to C_4H_5-N is one of the most sensitive reactions for both fuels. The reactions of C_5H_3O are especially important in the case of guaiacol: the termination reaction to form back cyclopentadienone is inhibiting, as it competes with the decomposition into smaller species, which constitutes a promoting pathway. The other inhibiting reactions shown in the sensitivity analyses concern reactions interchanging the four C_5 species involved in the inhibiting submechanism, constraining the decomposition into final products and slowing down flame propagation.

For both fuels and ϕ, it becomes apparent in the sensitivity analyses in Figure 4 that pathways leading to the above-described C_5 inhibiting submechanism have a promoting influence, even though this set of reactions inhibits the combustion process. For anisole, these reactions are A1O+O=P-C6H4O2+H and A1O=CO+C5H5, where para-benzoquinone (P-C6H4O2) and cyclopentadienyl radical respectively lead to a cyclopentadienol radical and cyclopentadienone (see Figure 2). These two channels compete with the two strongly inhibiting reactions of phenoxy radicals consuming the chain-branching H-atoms. In the same way, for guaiacol, the channel competing with the combination of hydroxyphenoxy with H-atoms and methyl radicals, OA1OH=CO+C5H4OH, has a promoting influence even through it leads to the C_5 inhibiting submechanism.

Figure 2 also shows important differences between the decomposition pathways of anisole under lean and rich conditions. Under rich conditions, unimolecular decomposition has an even higher contribution. Regarding the phenoxy radical decomposition, the reaction to para-benzoquinone becomes negligible, while the flows to cresols and cyclopentadienyl radical are amplified. At ϕ = 1.3, 83% of cyclopentadienone and 86% of C_5H_3O decompose into $C_{\leq 4}$ species, whereas these pathways represent only 50% and 69%, respectively, of their respective consumption in lean mixture. Therefore, the C_5H_XO submechanism becomes negligible under rich conditions, with a much lower sensitivity, as shown in Figure 4b. Under these conditions, the role of phenyl radicals becomes important. Its reactions, highlighted in the sensitivity analysis in Figure 4d, are at the heart of a competition between the

inhibiting termination reaction leading to benzene and promoting channels, notably the branching reaction, phenyl + O_2 giving phenoxy + O. Inhibiting pathways from the cyclopentadienyl radical are also highlighted in Figure 4c. They concern the termination reaction forming cyclopentadiene and the pathway C_5H_5 – cC_5H_4 – C_7H_6, composed of a disproportionation termination $C_5H_5+OH \rightarrow cC_5H_4+H_2O$ and the molecular reaction $cC_5H_4+C_2H_2 \rightarrow C_7H_6$ (inhibiting), in competition with $cC_5H_4+H \rightarrow C_5H_5$ (promoting).

3.2. JSR experimental and simulated results – Kinetic analysis

The guaiacol JSR oxidation experiments were performed under steady-state conditions at a constant pressure slightly above 1 atm (exactly 800 Torr), with temperatures ranging from 600 to 925 K, and ϕ of 0.5, 1, and 2. The initial fuel mole fraction was set at 0.005, with a high helium dilution to prevent excessive temperature gradients inside the reactor. Flow rates were adjusted at each temperature to achieve a residence time of τ = 2 s in the JSR.

This part first describes the experimental results obtained for guaiacol JSR oxidation and compares them with simulations using the COLIBRI v2 model. The second part presents flow rate analyses for fuel consumption at 775 K and 900 K to understand the formation of the main products. Finally, the third part focuses on flow rate analyses related to two minor products but usually not considered in kinetic models: 1,3-benzodioxole and 1,3-benzodioxole-2-one.

3.2.1. Experimental results in JSR for guaiacol oxidation

A total of 22 products were detected. Light products containing up to 5 carbon atoms include CO, CO_2, methane, ethylene, ethane, propene, acetaldehyde, 1,3 butadiene, 2,5-dihydrofuran, and 2-cyclopent-1-one. Heavy products containing more than 5 carbon atoms consist of benzene, toluene, phenol, benzaldehyde, benzofuran, 1,3-benzodioxole, 2-hydroxybenzaldehyde, pyrocatechol, anisole, styrene, 1,3-benzodioxole-2-one, and C_9H_8O. The last species might be cinnamaldehyde or indanone, but there is a very large uncertainty in the mass spectrometry identification according to the comparison with spectra in the NIST08 library. Figure S23 displays the experimental mole fractions of the three products that are not considered in the COLIBRI v2 model: 2,5-dihydrofuran, C_9H_8O, and 2-cyclopent-1-one.

Methylcatechol (with a maximum of up to 80 ppm), cresol (with a maximum of up to 27 ppm), and naphthalene (with a maximum of up to 2 ppm), which were detected by Nowakowska et al. [28], are not observed in the present work with no obvious reason. Conversely, 1,3-benzodioxole and 1,3-benzodioxole-2-one, which were identified here with reasonable certainty, were not reported by them. In their previous study, the structure of C_9H_8O could not be completely resolved. Even though 1-indanone and cinnamaldehyde were even injected in their GC, the obtained retention times did not match.

Figure 5 presents the calculated product selectivities at 725 K and 900 K. This figure indicates that the two major products at both temperatures, with a selectivity above 10%, are CO and CO_2. At 725 K, there is significant formation of oxygenated aromatics, with a selectivity of 2-hydroxybenzaldehyde close to 20% and a significant production of C_9H_8O, phenol, pyrocatechol, and benzodioxole. These species are the first intermediates in guaiacol decomposition at low temperatures. At 900 K, the CO selectivity reaches 70%, with a significant formation of hydrocarbons (ethylene, ethane, propene, 1,3-butadiene, benzene…), which constitute the secondary intermediates and final products.

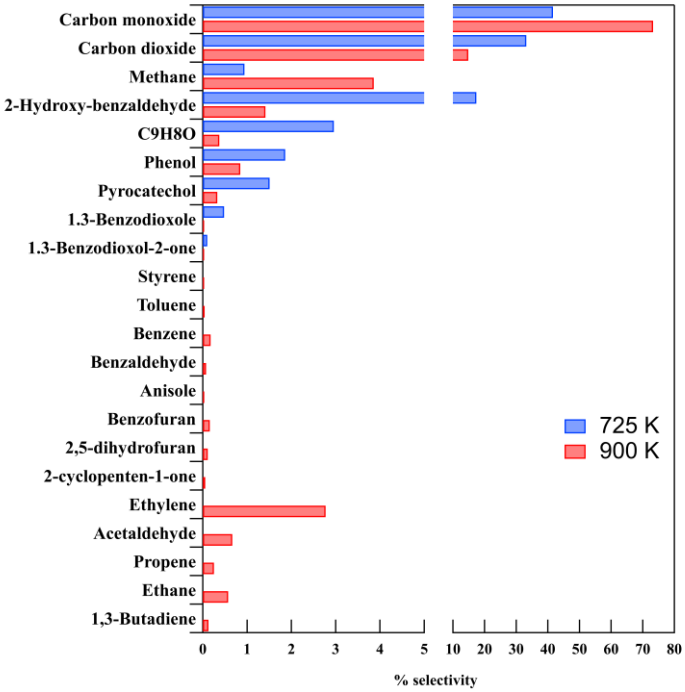

Figure 5: Product selectivity at 725 and 900 K (oxidation of guaiacol in a JSR at ϕ=1).

Figures S24 and S25 in SM display a comparison of our experimental data at ϕ = 1 against those of Nowakowska et al. [28], as well as simulations using their model and ours. Overall, there is good agreement between both sets of experimental data; the values of the fuel and mole fractions of products are close, except for pyrocatechol and phenol. It can be assumed that these differences might be explained by the wall treatment in our study, which was not conducted in the work of Nowakowska et al. [28].

Figure 6 shows the consumption of the fuel along with the O_2 mole fractions. This figure shows that the effect of ϕ on the fuel consumption is very limited. The consumption of the fuel and O_2 is well predicted by the kinetic model, regardless of the equivalence ratio.

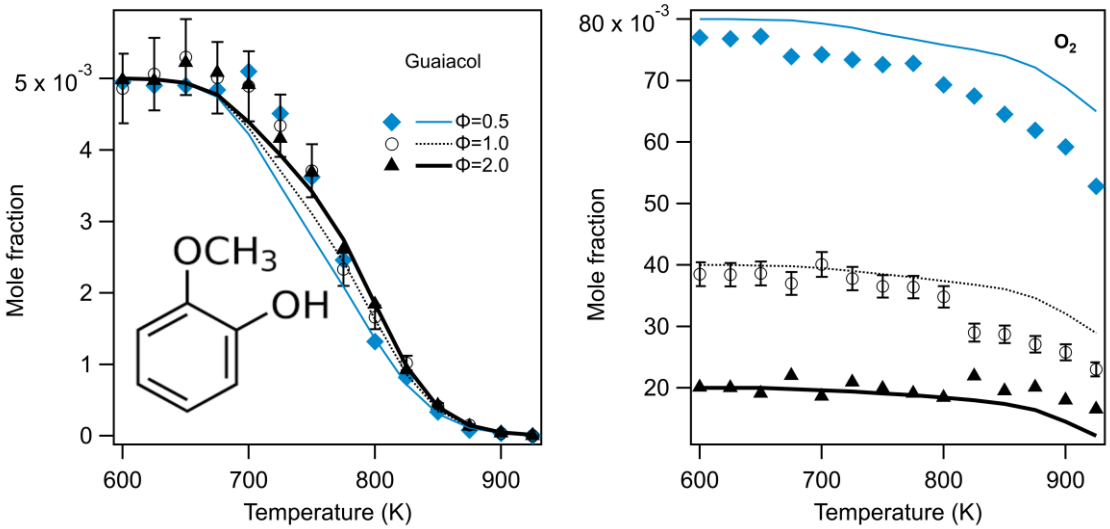

Figure 6: Mole fractions of fuel and oxygen vs. temperature (oxidation of guaiacol in a JSR). Symbols are experiments and line are simulations using the kinetic model. Error bars are only shown for ϕ=1.

Figure 7 shows a comparison between experimental and predicted mole fractions of CO, CO_2, C_1-C_4 hydrocarbons, and acetaldehyde. The shape of the temperature profile of these products is well simulated by the kinetic model, except for acetaldehyde, as in the work of Nowakowska et al. [28]. The underestimation of oxygen consumption and CO formation at $\phi = 1$ and 0.5 might indicate some missing reactions with O_2 in the model for the compounds derived from guaiacol. The ethylene mole fractions are underestimated by a factor of around 2, and those of acetaldehyde by a factor close to 100.

Figure 8 shows the comparison between experiments and predictions of the kinetic model for the aromatic products. Reasonable predictions by the COLIBRI v2 model are obtained for all these products, except for toluene, benzaldehyde, and 1-3-benzodioxole. A significant improvement is achieved in the simulation of phenol compared to that of Nowakowska et al. [28] (see Figure S25), where these mole fractions were significantly underpredicted.

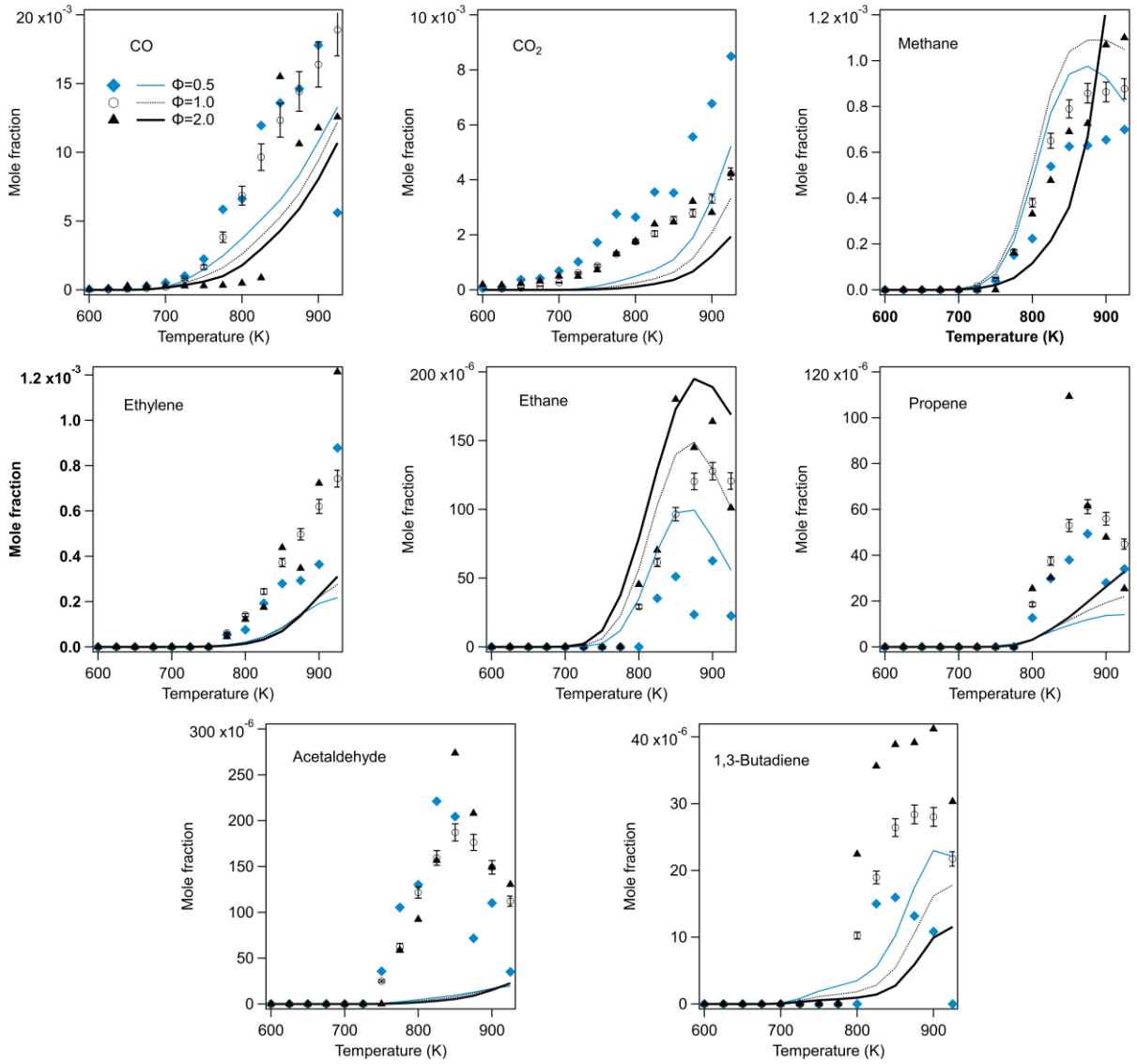

Figure 7: Mole fractions of light products vs. temperature (oxidation of guaiacol in a JSR). Symbols are experiments and line are simulations using the kinetic model. Error bars are only shown for ϕ=1.

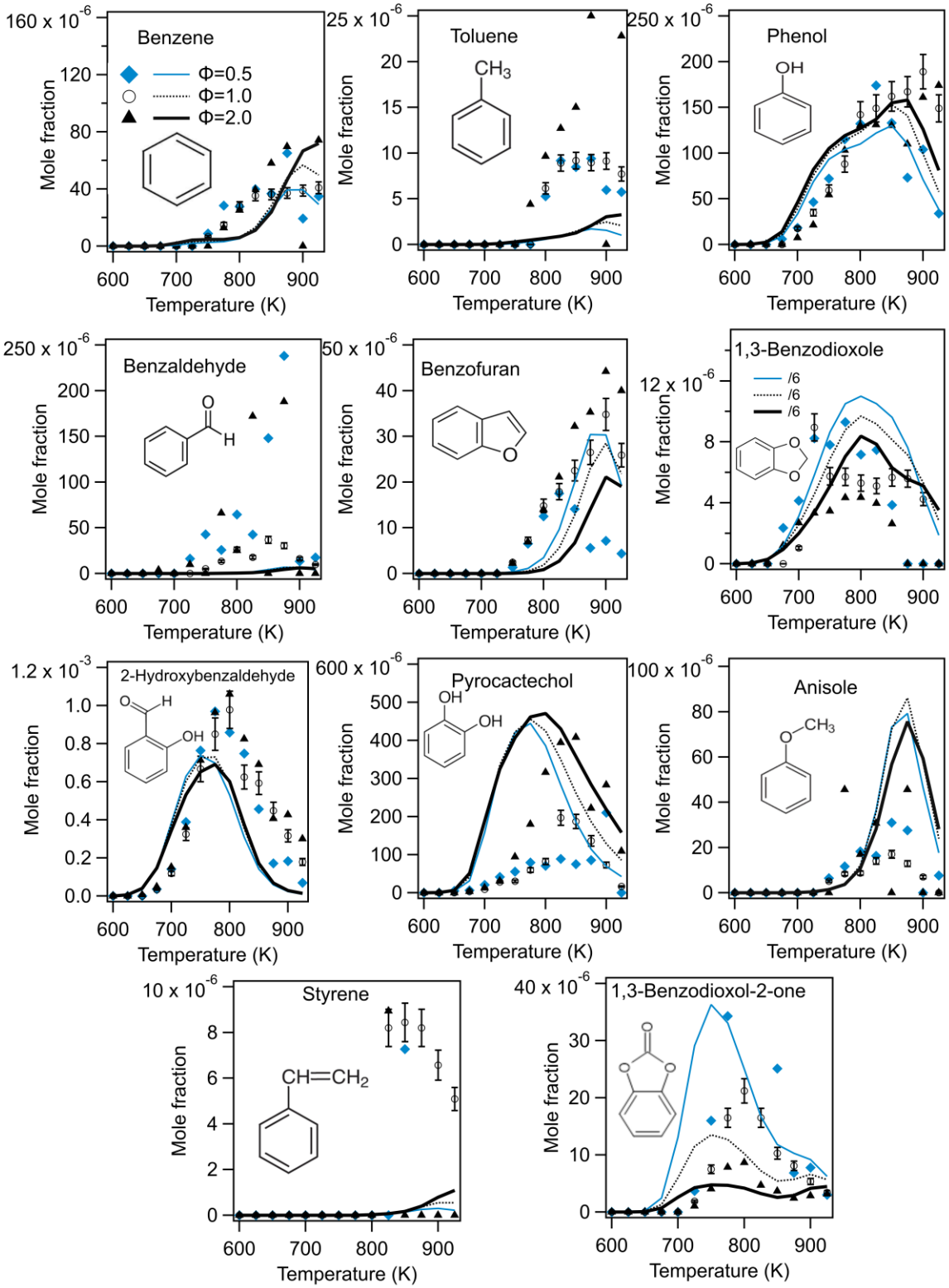

Figure 8: Mole fractions of heavy products considered in the kinetic model vs. temperature (oxidation of guaiacol in a JSR). Symbols are experiments and line are simulations. Error bars are only shown for ϕ=1.

Soot precursors were detected with notable mole fractions; this is the case of benzene (> dozens ppm for all equivalence ratios) as in Nowakowska et al. [28], as well as toluene and styrene. Nowakowska also quantified a low amount of naphthalene (up to 2 ppm), which was not detected in our study. The predictions of the new kinetic model are better for soot precursors than the model used in Nowakowska et al. [28], with a significant improvement concerning benzene and Nowakowska's naphthalene profile (see Figure S25). However, the measurements on PAHs have to be refined to be compare with those obtained in anisole oxidation, which seems to form more soot than in the case of guaiacol. This tendency is consistent with that given by the Yield Sooting Index (YSI): $YSI_{guaiacol} = 64$ and $YSI_{anisole} = 111$ [3].

It is particularly noticeable in the 1,3-benzodioxole and 1,3-benzodioxole-2-one profiles displayed in Figure 8 that these species are produced by a low-temperature pathway, around 750-800 K, and a high-temperature one above 900 K. 1,3-benzodioxole was already detected in our previous study on the oxidation of toluene and xylene isomers [29], with an acceptable simulation based on newly proposed pathway, which involves the addition of phenoxy radical to formaldehyde followed by a ring closure. Interestingly, the profile of 1,3-benzodioxole-2-one exhibits a stronger equivalence ratio dependence than that of 1,3-benzodioxole, which is likely the precursor of the former one via reactions involving oxygen, e.g. oxygen addition. Considering these observations and, given that the structure of 1,3-benzodioxole has strong similarities with that of guaiacol, new pathways displayed in Table S2 have been proposed to describe the formation and decomposition of these species. It can be seen in Figure 8 that the COLIBRI v2 model accurately reproduces the experimental mole fraction profiles with both low and high-temperature behaviors, even if some minor temperature shifts and an overestimation by a factor of 6 are observed for the benzodioxole mole fraction. The overestimation noted for this last product is certainly due to the fact that the related rate constants are based on analogies (see Table S2) and a better agreement might be obtained if those were derived from theoretical calculations. These deviations are acceptable considering the limited knowledge about the chemistry of these compounds. Furthermore, the large influence of ϕ on the formation of 1,3-benzodioxole-2-one is well simulated.

Concerning the possible formation of cinnamaldehyde (3-phenylpropenal), some pathways were envisaged. The combination of phenoxy and allyl resonance stabilized radicals and the combination of anisyl radicals and C_2 hydrocarbons followed by bicyclic intermediates, by analogy with what has been proposed for the isomerization of $C_6H_5OCH_2$ radical yielding $C_6H_5CH_2O$ radical [42], and then the formation of cinnamaldehyde. However, anisyl and phenoxy radicals are formed below 800 K, and the $C_{\leq 3}$ linear compounds only above 800 K, therefore the order of magnitude obtained numerically is far lower than that experimentally observed, about 100 ppm.

3.2.2. Flow rate analyses for guaiacol consumption

Figure 9 presents the flow analysis of guaiacol oxidation with the formation of the main detected aromatics in JSR at $\phi = 1$ and 775 K, corresponding to 50% of the fuel consumption. Contrary to what was shown for LBV (see Figure 3), the H-abstractions on both ramifications consume about half of guaiacol; the reactions involving phenylic H-atoms are negligible. The hydroxyanisyl radicals are formed both directly by H-abstractions and also by the isomerisation of the resonance-stabilized

methoxyphenoxy radicals. 94% of hydroxyanisyl radicals react through an anisyl rearrangement involving a three-membered ring, leading to radicals that decompose to yield hydroxybenzaldehyde, the most important quantified aromatic intermediate, and to a lesser extent, phenol. Other intermediates are directly formed from phenol like benzene, or after the formation of the phenoxy radical like anisole and benzofuran.

The other half of guaiacol is consumed through the unimolecular decomposition to form the hydroxyphenoxy radical, which leads to pyrocatechol, the second most important quantified aromatic intermediate, through a combination with H-atoms. The ipso-addition of H-atoms to a hydroxy group of pyrocatechol is another source of phenol (13% of phenol formation). Hydroxyphenoxy radicals also lead to ortho-benzoquinone and methylcatechol; both products were not detected here, however, the latter one was quantified by Nowakowska [28]. The H-abstractions of hydroxyl H-atoms from methylcatechol are not significant at 775 K, despite their importance for LBV.

A sensitivity analysis on guaiacol mole fraction at 675 K, at the very start of reactivity, is given in figure S26(a) in SM and shows a particularly large promoting effect of two particular reactions: the fuel unimolecular decomposition, and the H-abstraction by HO_2 on the hydroxy group. The influence of ϕ is less important for the unimolecular decomposition than for the H-abstractions, which are linked to the amount of hydroperoxy radicals formed through $H+O_2 \rightarrow HO_2$. At low temperature, H-atoms are produced through the beta-scission leading to hydroxybenzaldehyde. The start of this pathway is the H-abstractions from the fuel, which only slightly depends on ϕ as it is shown in Figure S27(a) presenting the first channels involved in the fuel decomposition at the start of its reactivity. Globally, the two sensitive pathways on the start of reactivity are independent of ϕ what explains the same start of reactivity whatever the equivalence ratio for guaiacol. On the same principle, Wagnon et al. [4] observed no influence of ϕ during the oxidation of anisole in a JSR, which is in agreement with Figure S26(b) in SM, showing that the start of reactivity is very sensitive to one particular reaction: the unimolecular decomposition of anisole. This reaction accounts for more than 80% of anisole consumption (see Figure S27(b)) and is independent of the equivalence ratio. So, in both cases, the independence on ϕ of the start of reactivity is mainly attributed to the unimolecular decomposition on the methoxy group.

A flow analysis of guaiacol oxidation at 900 K is given in Figure S28. At this temperature, the flow rate analysis is close to that for LBV, since 96% of the fuel unimolecularly decomposes, and the CO elimination to the cyclopentadienol radical becomes significant, representing 24% of hydroxyphenoxy radical consumption. At high temperature, the pathway from methylcatechol to phenoxy radical is crucial, as most aromatic intermediates are formed from phenoxy radicals at high temperatures. This pathway was neglected in the model of Nowakowska et al. [28] and has been amplified in the COLIBRI v2 model, leading to a significant improvement in the prediction of phenol, benzene, and benzofuran (see Figure S25). Ethylene and acetaldehyde, the two C_{4-} products the most underpredicted, are formed by the same pathways, from cyclopentadienone and, from ethane and propene, respectively, as in our recent simulations of the oxidation of toluene and xylenes isomers [29]. However, in this last

study, the model allowed reasonably predicting the JSR mole fractions of these two products. This might indicate formation pathways of these compounds specific of guaiacol and not considered in the Colibri v2 model.

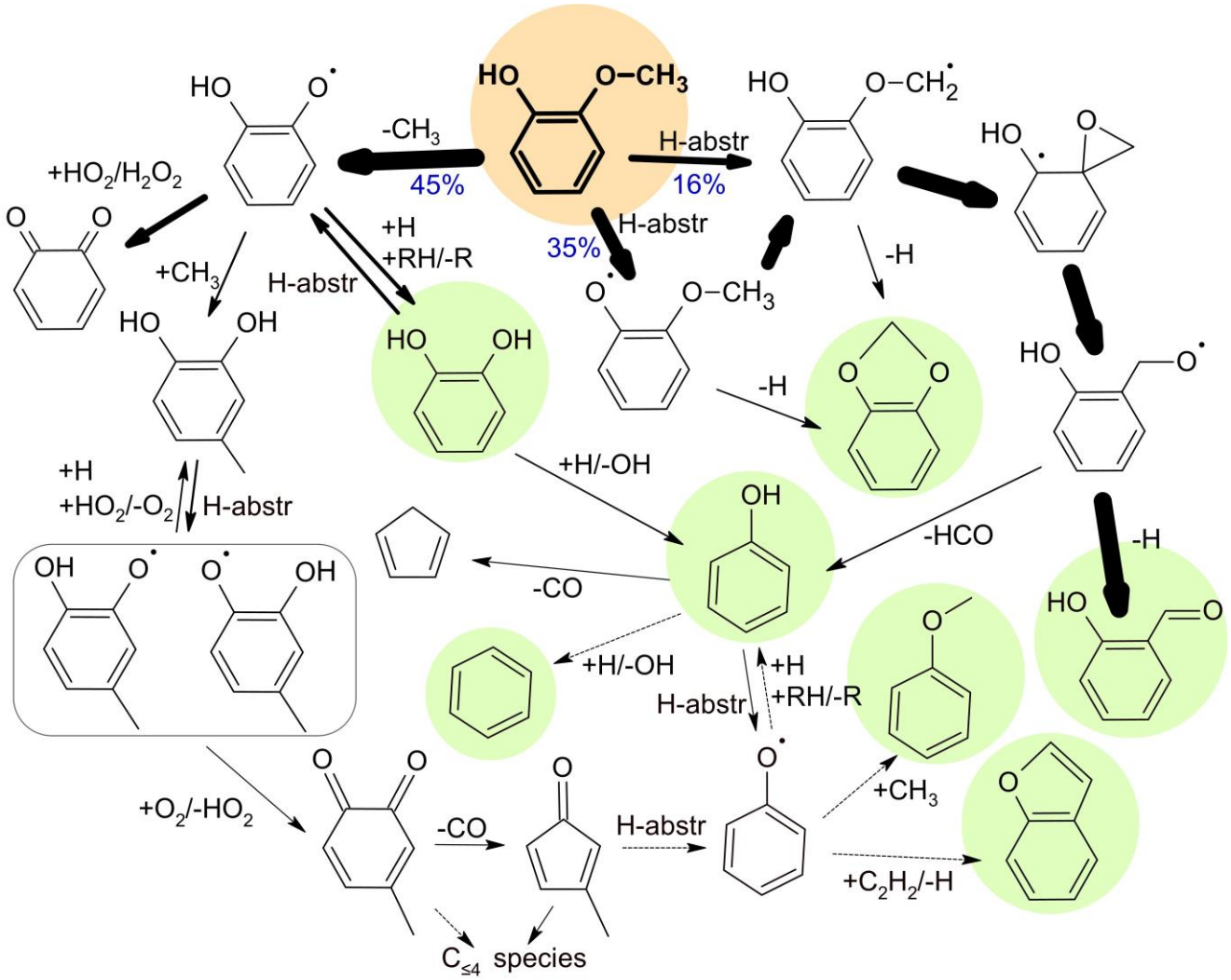

Figure 9: Flow analysis of guaiacol oxidation in JSR at 775K under stoichiometric conditions. Species highlighted in green are observed reaction products. Species highlighted in the box are the two radicals from methylcatechol (see text).

3.2.3. Flow rate analyses related to the formation and consumption of 1,3-benzodioxole and 1,3-benzodioxole-2-one

1,3-Benzodioxole and 1,3-benzodioxole-2-one are formed in low amounts, thus having a low impact on guaiacol reactivity; nevertheless, as those multi-oxygenated aromatic ethers are not usually seem amongst cyclic ethers produced during combustion [43], let us detail more their potential reaction pathways. The flow rate analyses of guaiacol consumption at 775 K (see Figure 9) and at 900 K (Figure S28) both indicate the formation of benzodioxole, a species newly detected in this study. The formation and decomposition pathways of 1,3-benzodioxole, and its related product, 1,3-benzodioxole-2-one, are

described in more details in the flow rate analysis in Figure 10 and are different at 900 K (see Figure 10 a) and at 725 K (see figure 10 b).

As shown in Figure S28, in JSR at 900 K, as it is observed in flame, guaiacol mainly decomposes through unimolecular decomposition leading to hydroxyphenoxy radicals, and through several steps to phenoxy radicals themselves. At this temperature (see Figure 10a), the formation of 1,3-benzodioxole occurs through the same pathway as during the oxidation of toluene and xylenes [29]: it is initiated by the addition of a phenoxy radical to formaldehyde and is followed by an internal ipso-addition on the aromatic cycle ($A1OCH_2O \rightarrow$Benzodioxole+H). Further reactions of 1,3-benzodioxole lead to 1,3-benzodioxole-2-one: H-abstractions followed by a combination with HO_2 radicals, decomposition of the hydroperoxide and finally, ketone formation. The degradation 1,3-benzodioxole-2-one is a source of CO_2.

At 725 K (see Figure 10b), 1,3-benzodioxole is obtained by a different channel, a ring closure between both ramifications in the methoxyphenoxy radical and hydroxyanisyl radical, both obtained by H-abstractions from guaiacol. The addition of O_2 on hydroxyanisyl radicals, followed by a beta-scission, leads to an ester product; H-abstractions on its both ramifications followed by a cyclization allow the formation of 1,3-benzodioxole-2-one. Note that at 725 K, it is the reverse reaction that forms 1,3-benzodioxole at 900 K that starts consuming it: the ipso-addition with H-atoms to give back $A1OCH_2O$ radicals (Benzodioxole+H$\rightarrow A1OCH_2O$). The decomposition pathways of 1,3-benzodioxole-2-one and 1,3-benzodioxole, both ultimately lead to a low-temperature production of CO_2.

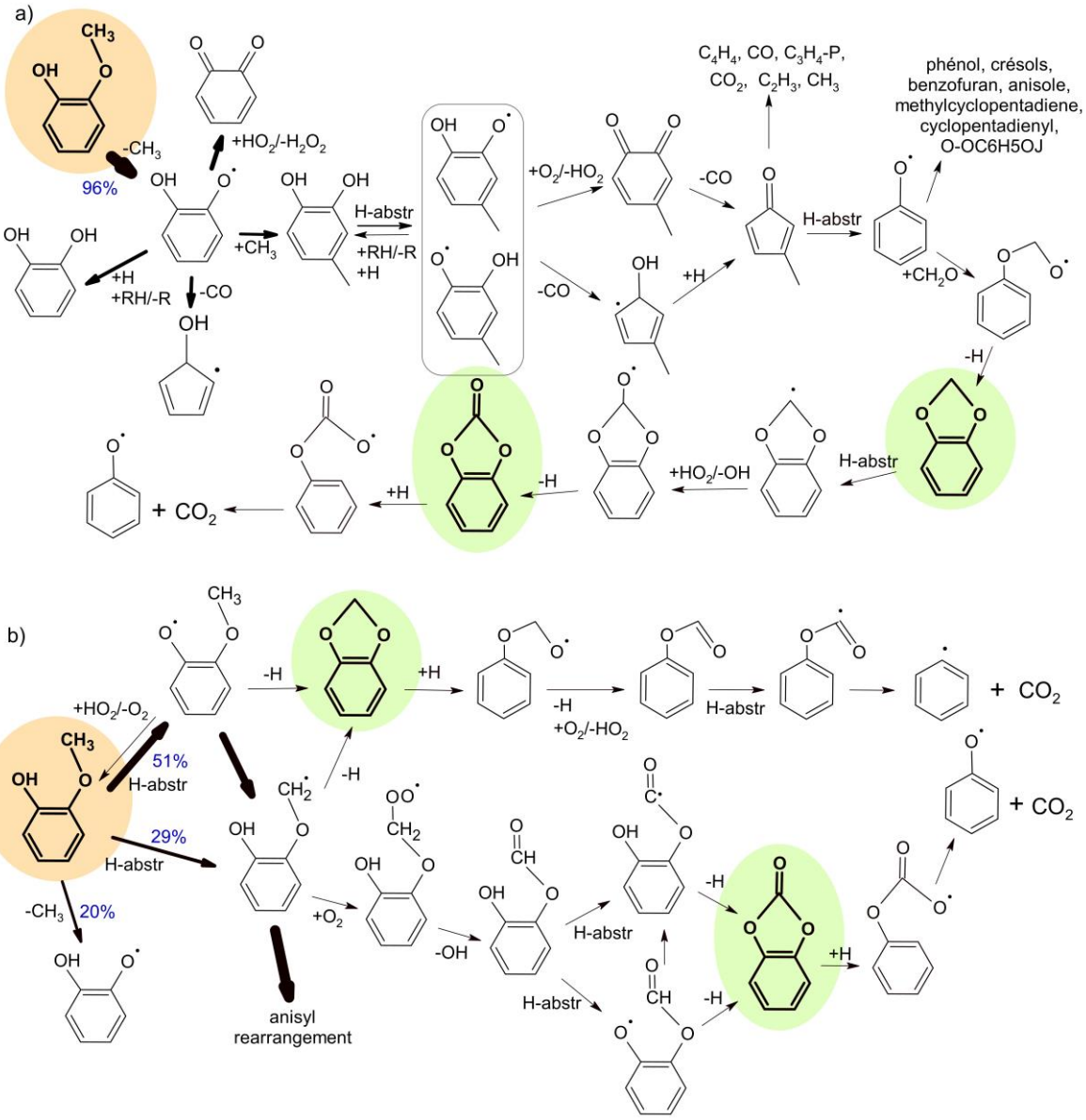

Figure 10: The formation and decomposition pathways of 1,3-benzodioxole and 1,3-benzodioxole-2-one at (a) 900 K and (b) 725 K.

4. CONCLUSIONS

The oxidation of guaiacol at low temperature has been investigated in a JSR over a wide range of temperatures (600-925 K) and at three equivalence ratios (0.5, 1, and 2). The experimental mole fractions of products have been recorded as functions of the experimental parameters, thanks to GC measurements, and were compared to mole fractions computed with a new kinetic model that has been developed in this work. The kinetic model has also been compared to adiabatic LBV measurements made using a flat flame burner for guaiacol and the archetypical case of anisole. The new kinetic model allows for satisfactory reproduction of both JSR and LBV measurements. Significant improvements in the predictions of some species such as phenols and benzene, have been obtained in this work compared

to the literature.

To better understand the combustion of guaiacol, it would be interesting to make measurements of LBV at higher fresh gas temperatures to overcome the volatility constraint and reach ϕ above 0.8. Furthermore, additional experimental data are still needed, such as ignition delay times and species profiles in a tubular reactor or in a flame, to build a comprehensive database.

Concerning the modeling part, future investigations using quantum chemistry on the reactions of C_5 oxygenated cyclic species, as well as on 1,3-benzodioxole and benzodioxole-2-one, should help to improve and complete the implemented pathways of those minor products in the kinetic model.

5. ACKNOWLEDGEMENTS

We acknowledge funding from the European Union's Horizon 2020 research and innovation program (BUILDING A LOW-CARBON, CLIMATE RESILIENT FUTURE: SECURE, CLEAN AND EFFICIENT ENERGY) under Grant Agreement No 101006744. The content presented in this document represents the views of the authors, and the European Commission has no liability in respect of the content.

6. REFERENCES

[1] Devi L, Ptasinski KJ, Janssen FJJG. A review of the primary measures for tar elimination in biomass gasification processes. Biomass and Bioenergy 2003;24:125–40. https://doi.org/10.1016/S0961-9534(02)00102-2.

[2] McKendry P. Energy production from biomass (part 1): overview of biomass. Bioresource Technology 2002;83:37–46. https://doi.org/10.1016/S0960-8524(01)00118-3.

[3] Battin-Leclerc F, Delort N, Meziane I, Herbinet O, Sang Y, Li Y. Possible use as biofuels of monoaromatic oxygenates produced by lignin catalytic conversion: A review. Catalysis Today 2023;408:150–67. https://doi.org/10.1016/j.cattod.2022.06.006.

[4] Wagnon SW, Thion S, Nilsson EJK, Mehl M, Serinyel Z, Zhang K, et al. Experimental and modeling studies of a biofuel surrogate compound: laminar burning velocities and jet-stirred reactor measurements of anisole. Combustion and Flame 2018;189:325–36. https://doi.org/10.1016/j.combustflame.2017.10.020.

[5] Zare S, Roy S, El Maadi A, Askari O. An investigation on laminar burning speed and flame structure of anisole-air mixture. Fuel 2019;244:120–31. https://doi.org/10.1016/j.fuel.2019.01.149.

[6] Wu Y, Rossow B, Modica V, Yu X, Wu L, Grisch F. Laminar flame speed of lignocellulosic biomass-derived oxygenates and blends of gasoline/oxygenates. Fuel 2017;202:572–82. https://doi.org/10.1016/j.fuel.2017.04.085.

[7] Büttgen RD, Tian M, Fenard Y, Minwegen H, Boot MD, Heufer KA. An experimental, theoretical and kinetic modelling study on the reactivity of a lignin model compound anisole under engine-relevant conditions. Fuel 2020;269:117190. https://doi.org/10.1016/j.fuel.2020.117190.

[8] Herzler J, Fikri M, Schulz C. Ignition Delay Time Study of Aromatic LIF Tracers in a Wide Temperature and Pressure Range 2017.

[9] Lin C-Y, Lin MC. Thermal decomposition of methyl phenyl ether in shock waves: the kinetics of phenoxy radical reactions. J Phys Chem 1986;90:425–31. https://doi.org/10.1021/j100275a014.

[10] Zabeti S, Aghsaee M, Fikri M, Welz O, Schulz C. Optical properties and pyrolysis of shock-heated gas-phase anisole. Proceedings of the Combustion Institute 2017;36:4525–32. https://doi.org/10.1016/j.proci.2016.06.156.
[11] Pelucchi M, Faravelli T, Frassoldati A, Ranzi E, SriBala G, Marin GB, et al. Experimental and Kinetic Modeling Study of Pyrolysis and Combustion of Anisole. Chemical Engineering Transactions 2018;65.
[12] Yuan W, Li T, Li Y, Zeng M, Zhang Y, Zou J, et al. Experimental and kinetic modeling investigation on anisole pyrolysis: Implications on phenoxy and cyclopentadienyl chemistry. Combustion and Flame 2019;201:187–99. https://doi.org/10.1016/j.combustflame.2018.12.028.
[13] Arends IWCE, Louw R, Mulder P. Kinetic study of the thermolysis of anisole in a hydrogen atmosphere. J Phys Chem 1993;97:7914–25. https://doi.org/10.1021/j100132a020.
[14] Pecullan M, Brezinsky K, Glassman I. Pyrolysis and Oxidation of Anisole near 1000 K. J Phys Chem A 1997;101:3305–16. https://doi.org/10.1021/jp963203b.
[15] Platonov VV, Proskuryakov VA, Ryl'tsova SV, Popova YuN. Homogeneous Pyrolysis of Anisole. Russian Journal of Applied Chemistry 2001;74:1047–52. https://doi.org/10.1023/A:1013076330586.
[16] Friderichsen AV, Shin E-J, Evans RJ, Nimlos MR, Dayton DC, Ellison GB. The pyrolysis of anisole (C6H5OCH3) using a hyperthermal nozzle. Fuel 2001;80:1747–55. https://doi.org/10.1016/S0016-2361(01)00059-X.
[17] Chen B, Kruse S, Schmid R, Cai L, Hansen N, Pitsch H. Oxygenated PAH Formation Chemistry Investigation in Anisole Jet Stirred Reactor Oxidation by a Thermodynamic Approach. Energy Fuels 2021;35:1535–45. https://doi.org/10.1021/acs.energyfuels.0c03829.
[18] Nowakowska M, Herbinet O, Dufour A, Glaude P-A. Detailed kinetic study of anisole pyrolysis and oxidation to understand tar formation during biomass combustion and gasification. Combustion and Flame 2014;161:1474–88. https://doi.org/10.1016/j.combustflame.2013.11.024.
[19] Mackie JC, Doolan KR, Nelson PF. Kinetics of the thermal decomposition of methoxybenzene (anisole). ACS Publications 1989. https://doi.org/10.1021/j100339a033.
[20] Bierkandt T, Hemberger P, Oßwald P, Krüger D, Köhler M, Kasper T. Flame structure of laminar premixed anisole flames investigated by photoionization mass spectrometry and photoelectron spectroscopy. Proceedings of the Combustion Institute 2019;37:1579–87. https://doi.org/10.1016/j.proci.2018.07.037.
[21] Chen B, Hellmuth M, Faller S, May L, Liu P, Cai L, et al. Exploring the combustion chemistry of anisole in laminar counterflow diffusion-flames under oxy-fuel conditions. Combustion and Flame 2021:111929. https://doi.org/10.1016/j.combustflame.2021.111929.
[22] Font Palma C. Modelling of tar formation and evolution for biomass gasification: A review. Applied Energy 2013;111:129–41. https://doi.org/10.1016/j.apenergy.2013.04.082.
[23] Jia L, Dufour A, Le Brech Y, Authier O, Mauviel G. On-line analysis of primary tars from biomass pyrolysis by single photoionization mass spectrometry: Experiments and detailed modelling. Chemical Engineering Journal 2017;313:270–82. https://doi.org/10.1016/j.cej.2016.12.021.
[24] Ceylan R, Bredenberg J. Hydrogenolysis and hydrocracking of the carbon-oxygen bond. 2. Thermal cleavage of the carbon-oxygen bond in guaiacol. Fuel (Guildford) 1982;61:377–82. https://doi.org/10.1016/0016-2361(82)90054-0.
[25] Vuori A. Pyrolysis studies of some simple coal related aromatic methyl ethers. Fuel 1986;65:1575–83. https://doi.org/10.1016/0016-2361(86)90335-2.
[26] Vuori AI, Bredenberg JB. Thermal chemistry pathways of substituted anisoles. Ind Eng Chem Res 2002:359–65. https://doi.org/10.1021/ie00062a031.
[27] Yerrayya A, Natarajan U, Vinu R. Fast pyrolysis of guaiacol to simple phenols: Experiments, theory and kinetic model. Chemical Engineering Science 2019;207:619–30. https://doi.org/10.1016/j.ces.2019.06.025.

[28] Nowakowska M, Herbinet O, Dufour A, Glaude PA. Kinetic Study of the Pyrolysis and Oxidation of Guaiacol. J Phys Chem A 2018;122:7894–909. https://doi.org/10.1021/acs.jpca.8b06301.
[29] Meziane I, Delort N, Herbinet O, Bounaceur R, Battin-Leclerc F. A comparative study of the oxidation of toluene and the three isomers of xylene. Combustion and Flame 2023;257:113046. https://doi.org/10.1016/j.combustflame.2023.113046.
[30] Bosschaart KJ, de Goey LPH. The laminar burning velocity of flames propagating in mixtures of hydrocarbons and air measured with the heat flux method. Combustion and Flame 2004;136:261–9. https://doi.org/10.1016/j.combustflame.2003.10.005.
[31] Dirrenberger P, Glaude PA, Bounaceur R, Le Gall H, da Cruz AP, Konnov AA, et al. Laminar burning velocity of gasolines with addition of ethanol. Fuel 2014;115:162–9. https://doi.org/10.1016/j.fuel.2013.07.015.
[32] Yu JF, Yu R, Fan XQ, Christensen M, Konnov AA, Bai XS. Onset of cellular flame instability in adiabatic CH4/O2/CO2 and CH4/air laminar premixed flames stabilized on a flat-flame burner. Combustion and Flame 2013;160:1276–86. https://doi.org/10.1016/j.combustflame.2013.02.011.
[33] Egerton AC, Warren DR. Kinetics of the hydrogen/oxygen reaction I. The explosion region in boric acid-coated vessels. Proceedings of the Royal Society of London Series A Mathematical and Physical Sciences 1997;204:465–76. https://doi.org/10.1098/rspa.1951.0003.
[34] Meziane I, Fenard Y, Delort N, Herbinet O, Bourgalais J, Ramalingam A, et al. Experimental and modeling study of acetone combustion. Combustion and Flame 2022:112416. https://doi.org/10.1016/j.combustflame.2022.112416.
[35] Stagni A, Song Y, Vandewalle LA, Van Geem KM, Marin GB, Herbinet O, et al. The role of chemistry in the oscillating combustion of hydrocarbons: An experimental and theoretical study. Chem Eng J 2020;385:123401. https://doi.org/10.1016/j.cej.2019.123401.
[36] Burke U, Metcalfe WK, Burke SM, Heufer KA, Dagaut P, Curran HJ. A detailed chemical kinetic modeling, ignition delay time and jet-stirred reactor study of methanol oxidation. Combustion and Flame 2016;165:125–36. https://doi.org/10.1016/j.combustflame.2015.11.004.
[37] Yuan W, Li Y, Dagaut P, Yang J, Qi F. Investigation on the pyrolysis and oxidation of toluene over a wide range conditions. II. A comprehensive kinetic modeling study. Combustion and Flame 2015;162:22–40. https://doi.org/10.1016/j.combustflame.2014.07.011.
[38] Kukkadapu G, Kang D, Wagnon SW, Zhang K, Mehl M, Monge-Palacios M, et al. Kinetic modeling study of surrogate components for gasoline, jet and diesel fuels: C7-C11 methylated aromatics. Proceedings of the Combustion Institute 2019;37:521–9. https://doi.org/10.1016/j.proci.2018.08.016.
[39] Johnson MS, Dong X, Grinberg Dana A, Chung Y, Farina DJr, Gillis RJ, et al. RMG Database for Chemical Property Prediction. J Chem Inf Model 2022;62:4906–15. https://doi.org/10.1021/acs.jcim.2c00965.
[40] Wang H, Frenklach M. Transport properties of polycyclic aromatic hydrocarbons for flame modeling. Combustion and Flame 1994;96:163–70. https://doi.org/10.1016/0010-2180(94)90167-8.
[41] Kee RJ, Rupley FM, Miller JA, Coltrin ME, Grcar JF, Meeks E, et al. CHEMKIN Collection, release 3.6; Reaction Design. Inc.; San Diego, CA, 2000.
[42] da Silva G, Bozzelli JW. Benzoxyl Radical Decomposition Kinetics: Formation of Benzaldehyde + H, Phenyl + CH_2O, and Benzene + HCO. J Phys Chem A 2009;113:6979–86. https://doi.org/10.1021/jp902458d.
[43] Tran L-S, Herbinet O, Carstensen H-H, Battin-Leclerc F. Chemical kinetics of cyclic ethers in combustion. Progress in Energy and Combustion Science 2022;92:101019. https://doi.org/10.1016/j.pecs.2022.101019.